A modified R^1◦xR^1 method for helioseismic rotation inversions

Pijpers, F. P.; Thompson, M. J.

DOI
10.1093/mnras/279.2.498
Publication date
1996

Published in
Monthly Notices of the Royal Astronomical Society

Mon. Not. R. Astron. Soc. **000**, 000–000 (1994) Printed 1 August 2021

A modified $\mathbb{R}^1 \otimes \mathbb{R}^1$ method for helioseismic rotation inversions

F. P. Pijpers[1,2] and M. J. Thompson[3]

[1] *Uppsala Astronomical Observatory, Box 515, S-751 20 Uppsala, Sweden*
[2] *Present address: Teoretisk Astrofysik Center, Danmarks Grundforskningsfond, Institut for Fysik og Astronomi, Aarhus Universitet, DK-8000 Aarhus C, Denmark*
[3] *Astronomy Unit, Queen Mary and Westfield College, University of London, Mile End Road, London E1 4NS, U.K.*

Accepted . Received

ABSTRACT

We present an efficient method for two dimensional inversions for the solar rotation rate using the Subtractive Optimally Localized Averages (SOLA) method and a modification of the $\mathbb{R}^1 \otimes \mathbb{R}^1$ technique proposed by Sekii (1993a,b). The SOLA method is based on explicit construction of averaging kernels similar to the Backus-Gilbert method. The versatility and reliability of the SOLA method in reproducing a target form for the averaging kernel, in combination with the idea of the $\mathbb{R}^1 \otimes \mathbb{R}^1$ decomposition, results in a computationally very efficient inversion algorithm. This is particularly important for full 2-D inversions of helioseismic data in which the number of modes runs into at least tens of thousands.

Key words: Sun : oscillations of – Sun : rotation of – Sun : structure of – Numerical methods

1 INTRODUCTION

The solar 5-minute oscillations can be described as a superposition of eigenmodes of non-radial pulsation. Each mode is identified by three integers (n, l, m), where l and m are the degree and order respectively of a spherical harmonic, and n is essentially the number of radial nodes in the displacement eigenfunction: m can take all values from $-l$ to $+l$. In a spherically symmetric, nonrotating star, the frequency of an eigenmode would be independent of m and thus there would be multiplets of $(2l + 1)$ modes with identical frequencies, each multiplet corresponding to an (n, l) pair. Rotation lifts this $(2l + 1)$-fold degeneracy. The difference in frequency between modes in the same multiplet is called the (rotational) frequency splitting. The frequency splitting is determined by the rotation rate inside the Sun and can be used in an inverse problem to probe the Sun's internal rotation. In particular, they enable one to perform 2-D inversions for the rotation rate as a function of radius and latitude.

Large helioseismic data sets should soon be available from various observational campaigns, notably the Global Oscillations Network Group (GONG) and MDI-SOI on board the SOHO satellite. To make optimal use of these data, the algorithms for full 2-D helioseismic inversions need to become efficient in handling several hundreds of thousands, or even millions, of data (modes) simultaneously. Optimally localized averages (OLA) techniques, which have proved very popular for 1-D helioseimic inversions involving only a few thousand data, require a matrix to be inverted whose order is the total number of data. This is prohibitively expensive computationally in the 2-D case – though one may be able to make the computation tractable by preprocessing to reduce the number of data to which the OLA is applied (Christensen-Dalsgaard et al. 1994). Least-squares techniques (e.g. Schou et al. 1994), which require a matrix to be inverted whose order is the number of base functions, are also expensive in the 2-D case, where one might want a discretization of e.g. 200 bins in radius and 100 in latitude which gives a matrix of order 2×10^4.

Sekii (1993a,b) has exploited the fact that the rotation kernels are nearly separable in radius r and colatitude θ to develop a so-called $\mathbb{R}^1 \otimes \mathbb{R}^1$ inversion technique in which the true kernels are approximated by ones which are exactly separable. This results in a problem where the order of the largest matrix one has to invert is only the number of (n, l)-multiplets, which is only a few thousand.

Here we propose a modification to Sekii's $\mathbb{R}^1 \otimes \mathbb{R}^1$ method, in which the small deviations from separability of the kernels are taken into account. The computational burden is the same as for Sekii's approach; hence it is just as efficient. Again the problem is reduced to a series of 1D inversions, for which we use the subtractive optimally localized averages (SOLA) method of Pijpers & Thompson (1992, 1994; hereafter PT1, PT2). The SOLA has the advantage over other 1D inversion methods that it is possibly to keep close control over the averaging kernels that it produces: this turns out to be important for the $\mathbb{R}^1 \otimes \mathbb{R}^1$ inversion, as we shall see below (cf. also Sekii 1994).

2 THE $\mathbb{R}^1 \otimes \mathbb{R}^1$ METHOD

In a spherically symmetric, nonrotating star, the frequency ω_{nl} of a spheroidal mode of oscillation of radial order n and degree l is independent of the mode's azimuthal order m, and the displacement eigenfunction is

$$\left(\xi_{nl}(r), L^{-1}\eta_{nl}\frac{\partial}{\partial\theta}, \frac{L^{-1}\eta_{nl}}{\sin\theta}\frac{\partial}{\partial\phi}\right) P_l^m(\cos\theta)e^{im\phi} \tag{1}$$

with respect to spherical polar coordinates (r, θ, ϕ): here ξ_{nl} and η_{nl} are calculable functions, given a solar model; $L = \sqrt{l(l+1)}$; and P_l^m is the Legendre function of degree l and order m.

For a slowly rotating star the frequencies also depend on m. According to linear perturbation theory, which is an excellent approximation for the Sun, the difference between frequencies of modes with the same values of n and l, but opposite m, is given in terms of the eigenfunctions of the nonrotating star by

$$\omega_{nlm} - \omega_{nl\,-m} \;= 2mD_{nlm}$$

where

$$D_{nlm} \;= = \int_{-1}^{1}\int_{0}^{1} K_{nlm}(r,\theta)\Omega(r,\theta)\mathrm{d}r\,\mathrm{d}\cos\theta\,. \tag{2}$$

Here and in the following, we have made the radial variable r dimensionless by dividing it by the surface radius.

An OLA inversion for the rotation amounts to finding coefficients $\{c_{nlm}(r_0,\theta_0)\}$ so that

$$\bar{\Omega}(r_0,\theta_0) \equiv \sum_{nlm} c_{nlm}(r_0,\theta_0)D_{nlm} = \int\int \sum c_{nlm}K_{nlm}\Omega\,\mathrm{d}r\,\mathrm{d}\cos\theta\,. \tag{3}$$

is a localized average of the actual rotation rate Ω near $r = r_0, \theta = \theta_0$. To find the coefficients with a naive application of OLA would require a matrix to be inverted whose size was the total number of observed eigenmodes i.e. all avaliable (n, l, m) combinations. This is prohibitively expensive with a very large mode set. This paper is concerned with finding suitable coefficients in a computationally less expensive way, by exploiting properties of the kernels K_{nlm}.

The K_{nlm} are given by

$$K_{nlm}(r,\theta) \;=\; F_1^{nl}(r)G_1^{lm}(\theta) \;+\; F_2^{nl}(r)G_2^{lm}(\theta)\,, \tag{4}$$

where

$$F_1^{nl} \;\equiv\; \rho(r)r^2\left[\xi_{nl}^2(r) - 2L^{-1}\xi_{nl}(r)\eta_{nl}(r) + \eta_{nl}^2(r)\right]/I_{nl} \tag{5}$$

$$F_2^{nl} \;\equiv\; \rho(r)r^2\left[\eta_{nl}^2(r)\right]/I_{nl}\,, \tag{6}$$

ρ being the density and and ξ_{nl}, η_{nl} the components of the displacement eigenfunction in the nonrotating star, and

$$I_{nl} \;=\; \int_0^1 \mathrm{d}r\,\rho r^2(\xi_{nl}^2 + \eta_{nl}^2)\,; \tag{7}$$

and

$$G_1^{lm} \;\equiv\; \frac{(l-|m|)!}{(l+|m|)!}(l+1/2)\left[P_l^m(u)\right]^2 \tag{8}$$

$$G_2^{lm} \;\equiv\; \frac{1}{2}L^{-2}(1-u^2)\frac{\mathrm{d}^2G_1^{lm}}{\mathrm{d}u^2} \tag{9}$$

$$u \;\equiv\; \cos\theta\,.$$

Note that our definition of η_{nl} differs from that used by Sekii (1993a) by a factor of L. The ratio of the amplitudes of our ξ_{nl} and η_{nl} is roughly the ratio of the vertical wavenumber to the horizontal wavenumber (since for p modes the waves are almost longitudinal): thus for p modes, which propagate more nearly vertically than horizontally except near their turning points, ξ_{nl} is larger in magnitude than η_{nl}. More quantitatively, using the simplest asymptotics, the ratio of the amplitudes of F_1^{nl} to F_2^{nl} is of order $\omega^2r^2/L^2c_S^2$ in the acoustic cavity of the mode, ω being the mode's frequency and c_S the local adiabatic sound speed. Although this is of order unity near the lower turning point, it is much larger than unity elsewhere in the acoustic cavity. The angular functions G_1^{lm}, G_2^{lm} are of similar magnitude, since the two derivatives of G_1^{lm} each produce a factor of L and these cancel the factor of L^{-2}. Hence, as Sekii (1993a,b) observed, the contribution from $F_2^{nl}G_2^{lm}$ is generally small compared to that from $F_1^{nl}G_1^{lm}$, and so the original problem can be approximated by the separable problem

$$D_{nlm} \;\equiv \frac{\omega_{nlm} - \omega_{nl\,-m}}{2m} \approx \int\int F_1^{nl}(r)G_1^{lm}(u)\,\mathrm{d}r\mathrm{d}u\,. \tag{10}$$

A further aspect is that G_1^{lm} is everywhere positive, whereas G_2^{lm} oscillates to both positive and negative values – increasingly so for larger values of $(l - |m|)$ – and this too helps make the integrated contribution from the $F_2^{nl}G_2^{lm}$ small in general.

The essence of Sekii's idea for exploiting the separability is as follows. (We shall work within the framework of SOLA, which is the 1D method we shall employ.) Firstly, for each l one seeks coefficients $\widetilde{c}_l^{\,m}(\theta_0)$ such that

$$\sum_{m=1}^{l}\widetilde{c}_l^{\,m}(\theta_0)G_1^{lm}(\theta) \;\approx\; \widetilde{T}_l(u-u_0)\,, \tag{11}$$

where $u_0 = \cos\theta_0$, and $\widetilde{T}_l(u-u_0)$ is some chosen target form that is peaked around $\theta = \theta_0$ and small elsewhere. (The means by which such coefficients may be sought is described in PT1, PT2.) Then

$$\begin{aligned}\sum_{m=1}^{l}\widetilde{c}_l^{\,m}(\theta_0)D_{nlm} &= \\ &= \iint F_1^{nl}\left(\sum_{m=1}^{l}\widetilde{c}_l^{\,m}(\theta_0)G_1^{lm}(\theta)\right)\Omega(r,\theta)\,\mathrm{d}r\mathrm{d}u \\ &\equiv \int F_1^{nl}(r)\langle\Omega\rangle_l^{(\theta_0)}(r)\,\mathrm{d}r\,,\end{aligned} \tag{12}$$

where $\langle\Omega\rangle_l^{(\theta_0)} \approx \int\widetilde{T}_l(u-u_0)\Omega(r,\theta)\,\mathrm{d}u$. The second and final step is then to choose further coefficients $c^{nl}(r_0)$ such that

$$\sum_{nl} c^{nl}(r_0)F_1^{nl}(r) \;\approx\; T(r-r_0) \tag{13}$$

where similarly $T(r-r_0)$ is a chosen target function that is localized about some radius, r_0. Now if $\widetilde{T}_l(u-u_0)$ were in

fact independent of l, so $\langle\Omega\rangle_l = \langle\Omega\rangle$ say, eqs. (12) and (13) would imply that

$$\sum_{nlm} c^{nl}(r_0)\widetilde{c}_l^m(\theta_0)D_{nlm} \approx \int \sum_{nl} c^{nl}(r_0)F_1^{nl}(r) \times \langle\Omega\rangle^{(\theta_0)}(r)\,\mathrm{d}r \equiv \langle\langle\Omega\rangle\rangle^{(r_0,\theta_0)}\,, \tag{14}$$

where $\langle\langle\Omega\rangle\rangle^{(r_0,\theta_0)} \approx \int\int T(r-r_0)\widetilde{T}(u-u_0)\Omega(r,\theta)\,\mathrm{d}r\mathrm{d}\theta$. This then completes the $\mathbb{R}^1 \otimes \mathbb{R}^1$ inversion.

There are some drawbacks to the simple $\mathbb{R}^1 \otimes \mathbb{R}^1$ procedure outlined above. One is that the linear combinations on the left-hand side of (11) need to be essentially independent of l. A practical matter is that choosing the angular target functions to be independent of l does not guarantee that $\sum \widetilde{c}_l^m(\theta_0)G_1^{lm}(\theta)$ will itself be independent of the degree. However, SOLA is better than other commonly-used methods in forcing the linear combination to accurately resemble a given form (Dziembowski et al. 1994, Sekii 1994). A second point is that, in making all the target functions independent of l and r_0, the angular resolution implied by (11) is the same at all target radii. But because we have many more m values for the shallowly penetrating high-degree modes than for the deeply penetrating modes of low degree, we should be able to achieve much better angular resolution in the outer layers of the Sun than in its deep interior. [This point was appreciated by Sekii (1993b); but one of the contributions of the present paper is to suggest how the angular resolution might be chosen appropriate to the target depth.] Thus we need to relax the restriction that the combinations of latitudinal kernels are independent of both degree and radial target. In order to preserve the property that the radial inversion can be treated as a 1-D inversion, we shall allow the target functions $\mathcal{T}_l$, and hence the coefficients $\widetilde{c}_l^m$, to depend on the radial as well as the latitudinal location of the target point. Thirdly, although it may well be an excellent approximation to neglect the $F_2^{nl}G_2^{lm}$ terms for most presently observed modes, we hope that forthcoming datasets will extend to even lower frequency low-degree modes, for which Sekii's approximation is less good. For this reason, we wish to include the $F_2^{nl}G_2^{lm}$ contribution to the kernels while retaining the advantage of the basic $\mathbb{R}^1 \otimes \mathbb{R}^1$ concept.

We therefore now introduce a modification to Sekii's method to take into account the $F_2^{nl}G_2^{lm}$ terms when trying to form a localized average. Specifically, in the latitudinal localization, we seek coefficients $\widetilde{c}_l^m(r_0,\theta_0)$ to minimize

$$\int_{-1}^{1}\left(\sum_{m=1}^{l}\widetilde{c}_l^m G_1^{lm} - \mathcal{T}_{G_1}(u-u_0)\right)^2 \mathrm{d}u + \beta_l^2\int_{-1}^{1}\left(\sum_{m=1}^{l}\widetilde{c}_l^m G_2^{lm} - \mathcal{T}_{G_2}(u-u_0)\right)^2 \mathrm{d}u + \mu\sum_{m\,m'}\mathbf{E}^{(l)}_{m\,m'}\widetilde{c}_l^m\widetilde{c}_l^{m'}\,. \tag{15}$$

Here

$$\mu \equiv \mu_0\left(\sum_{m\,m'}\mathbf{E}^{(l)}_{m\,m'}\right)^{-1}\,, \tag{16}$$

μ_0 being an adjustable parameter; $\mathbf{E}^{(l)}_{m\,m'}$ is a suitable error-covariance matrix (see below). Minimizing the error term and obtaining a well-localized kernel are opposing aims (e.g. CDST) and the error weighting parameters μ_0 are used to obtain a compromise between them. We simultaneously force the linear combinations of G_1^{lm} and of G_2^{lm} to resemble the chosen target functions $\mathcal{T}_{G_1}$ and $\mathcal{T}_{G_2}$, which depend on l, r_0 and θ_0; and β_l is an adjustable parameter that weights the relative importance of matching $\mathcal{T}_{G_1}$ and matching $\mathcal{T}_{G_2}$. It is convenient to define function vectors

$$\mathbf{F}^{nl} = \begin{pmatrix} F_1^{nl} \\ F_2^{nl}\end{pmatrix}, \quad \mathbf{G}^{lm} = \begin{pmatrix} G_1^{lm} \\ G_2^{lm}\end{pmatrix}\,, \tag{17}$$

and

$$\mathcal{G}^l \;=\; \sum_m \widetilde{c}_l^m(\theta_0)\mathbf{G}^{lm}, \quad \mathcal{T}_G^l = \begin{pmatrix}\mathcal{T}_{G_1}\\ \mathcal{T}_{G_2}\end{pmatrix}\,. \tag{18}$$

Note that we shall generally omit the superscript l on $\mathcal{G}^l$ and $\mathcal{T}_G^l$, except when we wish to emphasize their dependence on the degree l. Then expression (15) can be written in suggestive form

$$\int_{-1}^{1}\mathrm{d}u\,(\mathcal{G}\;-\;\mathcal{T}_G)^T\begin{pmatrix}1 & 0\\ 0 & \beta_l^2\end{pmatrix}(\mathcal{G}\;-\;\mathcal{T}_G) \;+\; \mu\sum_{m\,m'}\mathbf{E}^{(l)}_{m\,m'}\widetilde{c}_l^m\widetilde{c}_l^{m'}\,. \tag{19}$$

In effect, we are seeking to localize a vector of functions rather than a single function, so that the inversion can once again be carried out as a sequence of two 1-D inversions but without the approximation Sekii (1993a,b) employed.

If a clean two-dimensional localization is finally to be achieved, it is desirable that the components $\mathcal{T}_{G_1}$ and $\mathcal{T}_{G_2}$ of $\mathcal{T}_G$ should have similar shapes. Thus we choose to make the second component the same as the first, up to a multiplicative scalar.

For convenience later we also impose an exact constraint on the first component of $\mathcal{G}$, that it be normalized such that

$$\int_{-1}^{1}\mathrm{d}u\;\mathcal{G}_1^l(\theta_0,\theta) \;=\; 1\,. \tag{20}$$

If the latitudinal localization is successful, then

$$\begin{aligned}\sum_{m=1}^{l}\widetilde{c}_l^m(r_0,\theta_0)D_{nlm} \;&=\int\int\mathbf{F}^{nl}\cdot\mathcal{G}\Omega(r,\theta)\,\mathrm{d}r\mathrm{d}u\\ &\approx\int\int\mathbf{F}^{nl}\cdot\mathcal{T}_G\Omega(r,\theta)\,\mathrm{d}r\mathrm{d}u\\ &=\int\int(F_1^{nl}+\zeta^{nl}F_2^{nl})\,\mathcal{T}_{G_1}\,\Omega\,\mathrm{d}r\,du\,,\end{aligned} \tag{21}$$

where ζ^{nl} is essentially the ratio of $\mathcal{T}_{G_2}$ to $\mathcal{T}_{G_1}$.

The second and final step in the two dimensional inversion is to find a second set of coefficients such that :

$$\mathcal{F}(r_0,r) \equiv \sum_{nl} c^{nl}(r_0)\left[F_1^{nl}(r)+\zeta^{nl}F_2^{nl}(r)\right] \tag{22}$$

is peaked around $r=r_0$ and is small everywhere else.

Actually the ζ^{nl} that enters in (22), which is defined explicitly below in equation (29), is not precisely the ratio

of the components of the latitudinal target function we use, though they are closely related. For our latitudinal localization we use

$$\mathcal{T}_G^l = \begin{pmatrix} \frac{1}{f_\theta \Delta_\theta} \exp\left[-\left(\frac{u-u_0}{\Delta_\theta}\right)^2\right] \\ \\ \frac{-1}{f_\theta \Delta_\theta^3 L^2} \exp\left[-\left(\frac{u-u_0}{\Delta_\theta}\right)^2\right] \end{pmatrix} . \tag{23}$$

The factor f_θ is a normalization factor which is included to make the total integral of $\mathcal{T}_{G1}$ equal to unity.

The radial target function is

$$\mathcal{T}_F = \frac{1}{f_r \Delta_r} \exp\left[-\left(\frac{r-r_0}{\Delta_r}\right)^2\right] \tag{24}$$

The expression to minimize is now

$$\int_0^1 \mathrm{d}r \, (\mathcal{F} - \mathcal{T}_F)^2 + \mu \sum_{nln'l'} \mathbf{E}_{nl\,n'l'} c^{nl} c^{n'l'} . \tag{25}$$

The free parameters Δ_r, Δ_θ should in general be functions of target position. The choice of Δ_r, Δ_θ at different radii and at different latitudes is an important issue. We have used the natural scaling that was presented in PT2 (cf. Thompson 1993) for radial and latitudinal resolution:

$$\begin{aligned} \Delta_r(r_0) &= \frac{\alpha_r}{8} \frac{c_S(r_0)}{R\nu_{\max}} \\ \Delta_\theta(r_0,\theta_0) &= \alpha_\theta \frac{\Delta_r}{r_0} \sqrt{1+\epsilon-u_0^2} \end{aligned} \tag{26}$$

where α_r and α_θ are constants of proportionality, independent of radius. To avoid problems at $u_0 = 1$ we include the small number $\epsilon = 0.075$. The strategy is to optimize the target widths at one target location and then use the relation (26) to calculate the target widths for all other locations. One should note that it is at this point that the dependence of the angular resolution on radius is introduced. The choice of functional dependence in (26) expresses the fact that one expects the attainable physical horizontal resolution and radial resolution to be very similar at all radii.

The factor ζ^{nl} that appears in the radial inversions (22) is necessary because the values of the two latitudinal averaging kernels at the location of their maxima differs due to the relation (9). The factor ζ^{nl} can compensate for this in the radial inversions so that in the final reconstructions the F_2^{nl} do not suddenly acquire a much smaller or larger weight due to the multiplication by the G_2^{lm}. Using (9) and (23) the ratio of the values of the two latitudinal kernels at their maximum is approximately :

$$\frac{\mathcal{G}_2(\theta_0, \theta=\theta_0)}{\mathcal{G}_1(\theta_0, \theta=\theta_0)} = -\frac{(1-u_0^2)}{\Delta_\theta^2 L^2} \tag{27}$$

The dependence of ζ^{nl} on the latitudinal resolution width implies that a straightforward application of this recipe means that the radial kernels to be used in the inversion depend on the choice of the target localization radius. This would defeat the purpose of using SOLA, because it would require calculating and inverting a new matrix for each new target position r_0. However, one can make use of the fact that any mode will be used primarily at target radii r_0 close to the turning point of that mode r_t. In other words the coefficient for this mode is only large if the averaging kernel to be constructed peaks near the turning point of that mode. Using this information and the scaling law for the latitudinal resolution widths, ζ^{nl} becomes :

$$\zeta^{nl} \propto \frac{\mathcal{G}_2(\theta_0, \theta=\theta_0)}{\mathcal{G}_1(\theta_0, \theta=\theta_0)} \sim -\left(\frac{4}{\pi \alpha_\theta \alpha_r} \frac{\nu_{\max}}{\nu}\right)^2 \tag{28}$$

If the absolute value of this factor is allowed to become much larger than unity it turns out to over-compensate for the effect of the amplitude of $\mathcal{G}_2$ in the radial inversion. Essentially what we wish to do with ζ^{nl} is to make sure that the product $F_2 G_2$ will indeed be treated as a small correction term, and hence ζ^{nl} should be less than unity. Thus in practice we achieve this while retaining the ν-dependence in (28) by defining

$$\zeta^{nl} = -\left(\frac{\nu_{\min}}{\nu}\right)^2 . \tag{29}$$

Equation (29) is used for all except the lowest degree modes for which the turning point is not close to the point at which the mode is actually used in localized kernels.

The factors β_l are used to compensate for the difference in the absolute value of the integrals of $\mathcal{T}_{\mathcal{G}_1}$ and $\mathcal{T}_{\mathcal{G}_2}$. We take $\beta_l = \langle \Delta_\theta^2 L^2 \rangle$ where the $\langle\rangle$ denotes a simple average over the latitudinal target points.

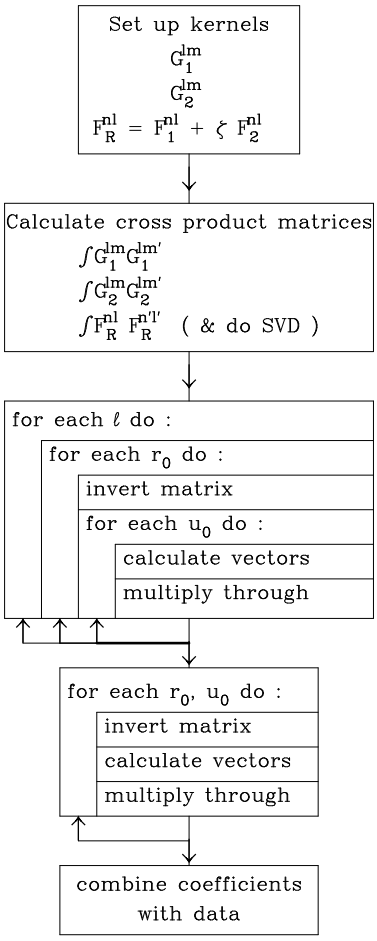

Figure 1 Flowchart showing the principal steps in the modified $\mathbb{R}^1 \otimes \mathbb{R}^1$ method presented here.

Now combining (21) with (22), this time keeping track of data errors ϵ_{nlm}, yields :

$$\sum_{nl} c^{nl}(r_0) \sum_m \widetilde{c}_l^m(r_0,\theta_0) D_{nlm} \;\approx$$

$$\approx \int_0^1 \mathrm{d}r \sum_{nl} c^{nl} \left[F_1^{nl}(r) + \zeta^{nl} F_2^{nl}(r)\right] \langle \Omega(r,\theta_0)\rangle^l + \\ + \sum_{nl} c^{nl} \sum_m \widetilde{c}_l^m \epsilon_{nlm} \; .$$

$$= \int_0^1 \mathrm{d}r\, \mathcal{F}(r_0,r) \langle \Omega(r,\theta_0)\rangle \; + \sum_{nl} c^{nl} \sum_m \widetilde{c}_l^m \epsilon_{nlm} \; .$$

$$= \; \langle \Omega(r_0,\theta_0)\rangle \; + \sum_{nl} c^{nl} \sum_m \widetilde{c}_l^m \epsilon_{nlm} \; . \qquad (30)$$

The constraint

$$\int_0^1 \mathrm{d}r\, \mathcal{F}(r_0,r) \;=\; 1 \qquad (31)$$

is now sufficient to ensure that the complete 2-D averaging kernel that is constructed is correctly normalized :

$$\int_0^1 \mathrm{d}r \int_{-1}^1 \mathrm{d}u \; \mathcal{K}(r_0,\theta_0;r,\theta) \;=\; 1 \; . \qquad (32)$$

where

$$\mathcal{K}(r_0,\theta_0;r,\theta) \equiv \sum_{nl} c^{nl} \sum_m \widetilde{c}_l^m \left[F_1^{nl} G_1^{lm} + F_2^{nl} G_2^{lm}\right] . \qquad (33)$$

The difference between the target form and the actually constructed kernel will give rise to a 'systematic' error a measure of which is χ :

$$\chi \equiv \int_0^1 \mathrm{d}r \int_{-1}^1 \mathrm{d}u \left[\sum_{nl} \sum_m c^{nl} \widetilde{c}_l^m \left(F_1^{nl} G_1^{lm} + F_2^{nl} G_2^{lm}\right) \right. \\ \left. - \mathcal{T}_F \mathcal{T}_{G1} \right]^2 \qquad (34)$$

The error covariance matrix $\mathbf{E}^{(l)}_{m\,m'}$ used in (15) and (19) is derived from that of the observed frequencies. Since the localization in colatitude is done at fixed l, the indices m and m' run over the range of m, viz from 1 to l. The appropriate covariance matrix is therefore $E_{nlm,nlm'}$ where l is the degree under consideration and n can be any order such that the (n,l) multiplet is in the dataset. The overall magnitude of E is irrelevant, since this is taken out by the scaling in μ. One should note that the error covariance of m and m' for a given l is taken to be independent of the value of n. This restricts the permitted data error covariance matrices. Of course one can proceed even if the errors do not satisfy this assumption, but the inversion will be less "optimal".

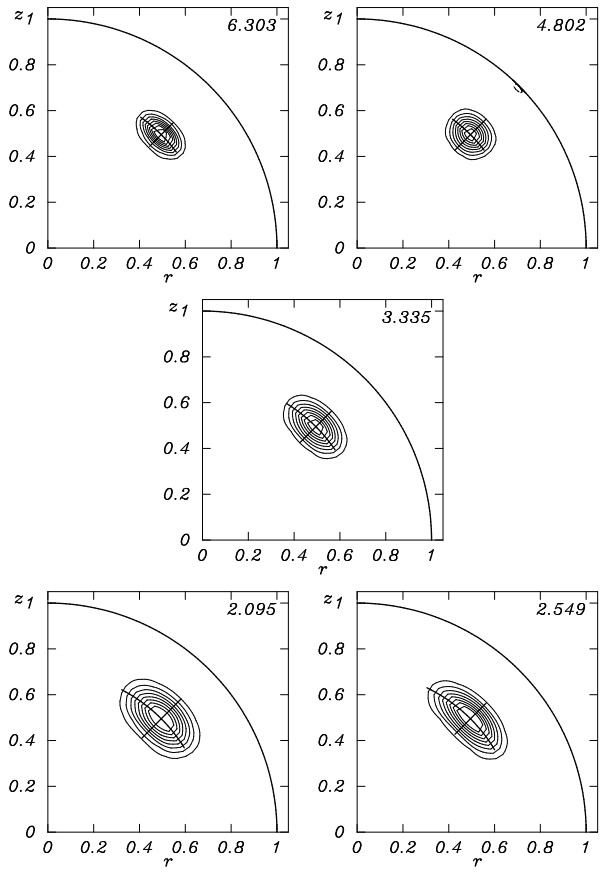

Figure 2 Constructed unimodular averaging kernels for various values of latitudinal and radial resolution widths. Each panel is labelled with the associated error in the solution, in nHz. Middle panel $\alpha_r = 8.0$, $\alpha_\theta = 1.5$. Upper left $\alpha_r = 6.0, \alpha_\theta = 1.5$, upper right $\alpha_r = 8.0, \alpha_\theta = 1.0$, lower left $\alpha_r = 10.0, \alpha_\theta = 1.5$, lower right $\alpha_r = 8.0, \alpha_\theta = 2.0$. The target location is $r_0 = 0.7R, \theta_0 = 45^\circ$ in all cases. The highest contour is $\sim 10\%$ below the peak value and the other contours are spaced in 1/8 of that value. The crossbar has an extension that corresponds that of a Gaussian at the lowest contour level which is at $|r - r_0| = 1.478\Delta_r$, $|u - u_0| = 1.478\Delta_\theta$. All error weighting parameters $\mu_0 = 0.1$

The error covariance matrix $\mathbf{E}_{nl\,n'l'}$ in the radial inversion is also derived from that of the observed frequencies. We assume that the data error covariance matrix can be factorised, into an error (co-)variance between multiplets and an error (co-)variance for m given any fixed l. If this is not in fact the case, one can still approximate the errors in this manner, but once again the inversion will presumably not be optimal. In the radial inversions the matrix $E_{nl\,n'l'}$ is obtained by :

$$E_{nl\,n'l'} \;=\; e_{nl\,n'l'} \left(\sum_{m\,m'} \mathbf{E}^{(l)}_{m\,m'} \widetilde{c}_l^m \widetilde{c}_l^{m'} \right)^{1/2} \times \\ \left(\sum_{m\,m'} \mathbf{E}^{(l')}_{m\,m'} \widetilde{c}_{l'}^m \widetilde{c}_{l'}^{m'} \right)^{1/2} \; . \qquad (35)$$

Here $e_{nl\,n'l'}$ is a matrix which expresses the error variance/ co-variance for all (n,l)-multiplets. We conclude this pre-

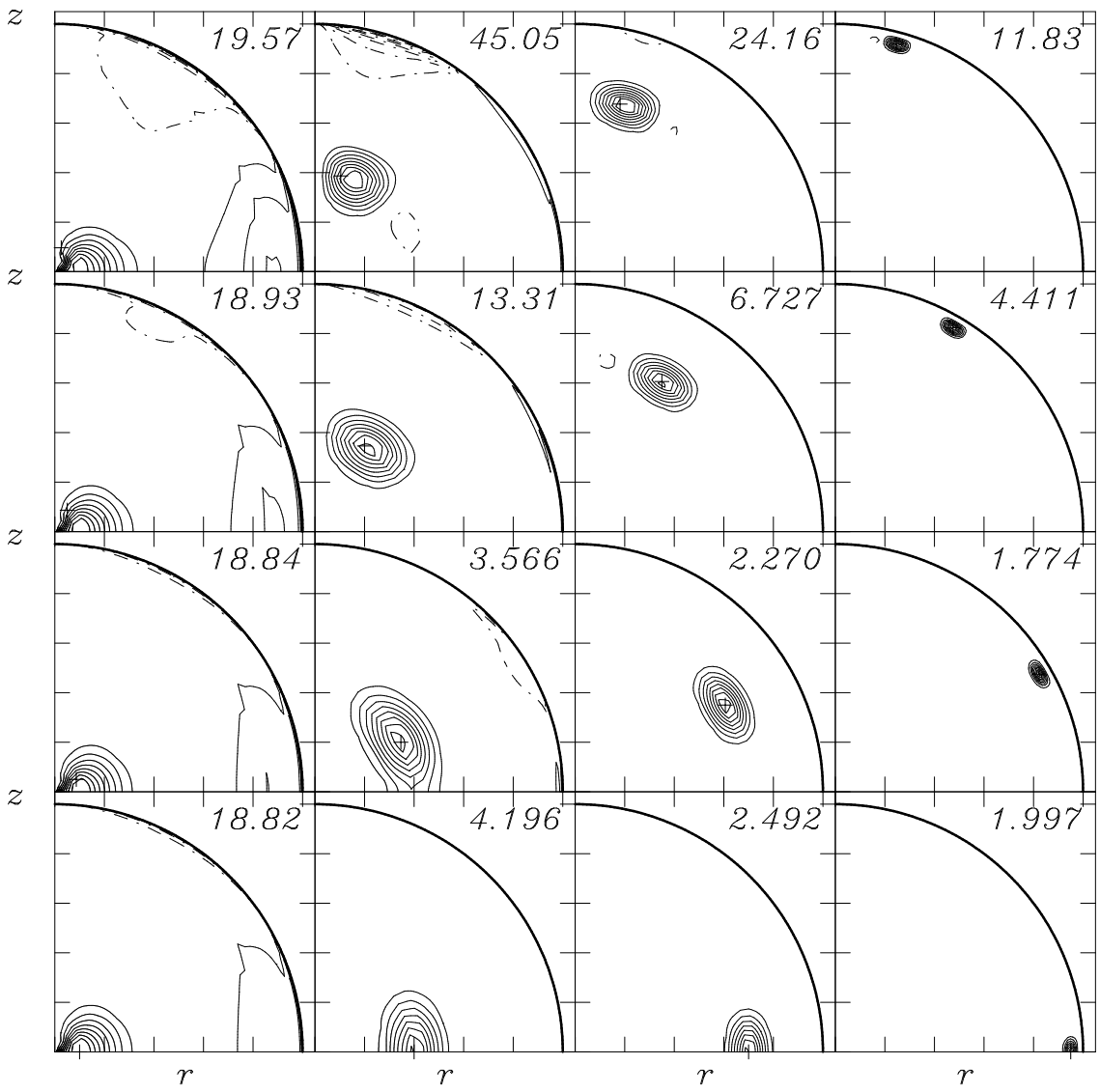

Figure 3 Unimodular averaging kernels at radii $r_0 = 0.1, 0.4, 0.7, 0.95$ and co-latitudes $\theta_0 = 15°, 30°, 60°, 90°$. Target locations are indicated by crosses; standard errors are as quoted. Localization parameters were $\alpha_r = 8.0$ $\alpha_\theta = 1.5$ and error weighting factor $\mu_0 = 0.1$ for all kernels.

sentation of the modified $\mathbb{R}^1 \otimes \mathbb{R}^1$ method by outlining the principle steps in a flow chart (Fig. 1). The first and second box represent steps that are preparatory to the actual inversion, the third box represents the latitudinal part of the inversion and the fourth box the radial part. The final box represents the process of combining the linear coefficients from the inversion with the data.

3 RESULTS

To illustrate the results which may be obtained with the method, we have applied it to artificial splitting data. The modeset is exactly the same as used in the GONG Hare and Hounds exercise (Gough & Toomre 1993): in brief, the set consists of f and p modes below 5mHz with

$$l = 1, 2, \ldots, 16, 18, \ldots, 50, 55, \ldots, 150, 160, \ldots, 250$$

making a total of 69662 individual modes with positive m values (in 1380 n, l multiplets). The assumed uncertainties on the frequency differences $\omega_{nlm} - \omega_{0nl}$ were of the form $\sigma_l(\nu) \equiv f(\nu)g(l)$, the functions f and g being estimated from Fig. 3.5 of Gough & Toomre (1993), and so are roughly the same as the assumed uncertainties in the Hare and Hounds exercise. The range of $\sigma_l(\nu)$ was from about 4nHz at low degree and frequency to roughly 700nHz at high degree and frequency. Note that under these assumptions, the uncertainties in the D_{nlm} are $f(\nu_{nl})g(l)/m$.

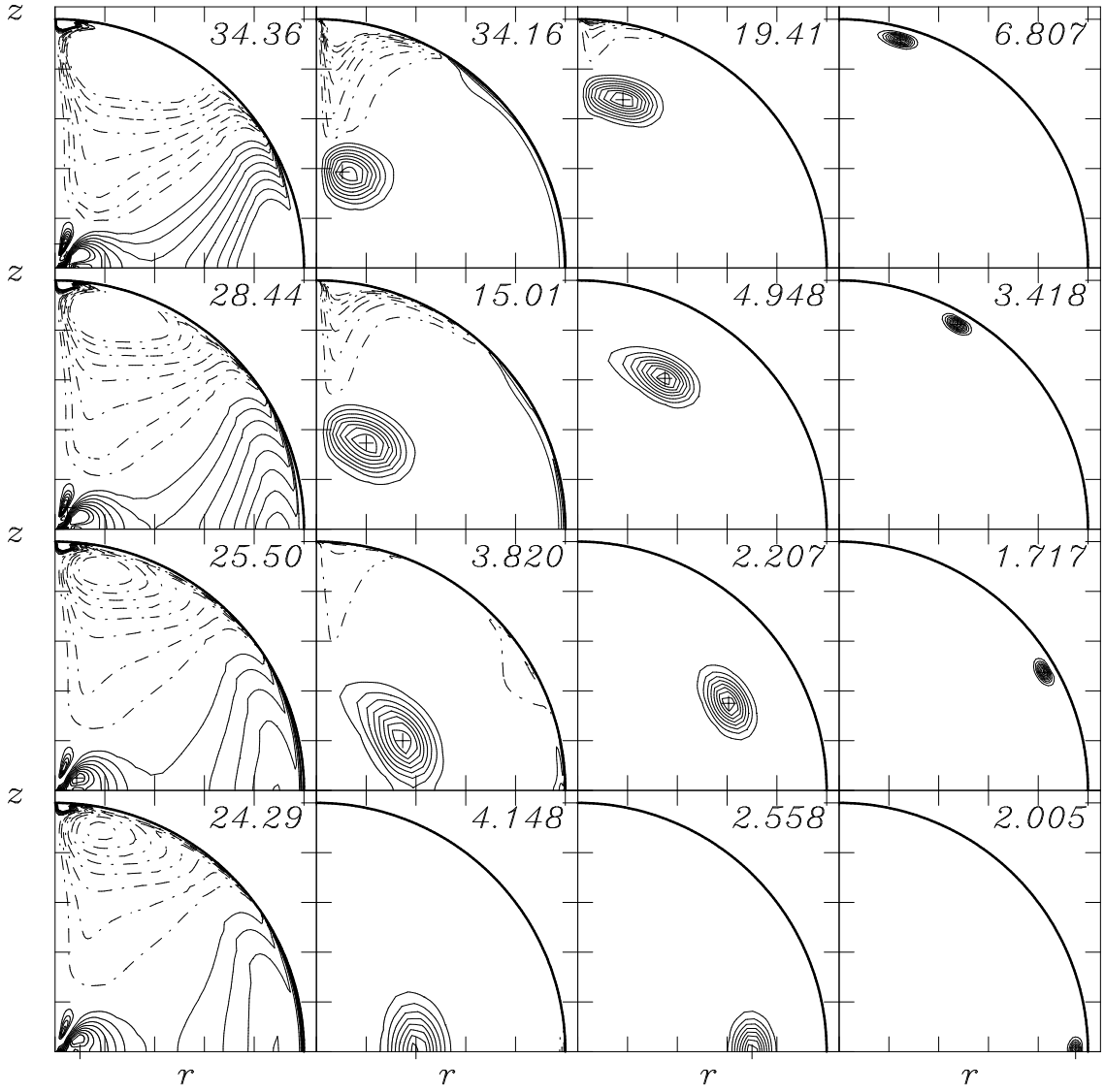

Figure 4 Unimodular averaging kernels at radii $r_0 = 0.1, 0.4, 0.7, 0.95$ and co-latitudes $\theta_0 = 15°, 30°, 60°, 90°$, without also localizing the F_2G_2-terms. Target locations are indicated by crosses; standard errors are as quoted. Trade-off parameter values are the same as for Fig. 3

It should be noted that the GONG Hare and Hounds dataset contains some low frequency p and f modes for which the assumptions about the location of the lower turing point made in the previous section are inaccurate or inappropriate. Specifically, for f modes with $l < 13$ and and also for the $l = 1, n = 1$ p mode, ζ^{nl} is computed using (27) and (26) with r_0 set to 0.1 instead of the turning point radius r_t.

The resolution and localization achieved in the inversions can be seen by inspecting the averaging kernels $\mathcal{K}(r_0, \theta_0; r, \theta)$, defined in equation (33). In Fig. 2 we illustrate averaging kernels at $r_0 = 0.7R$, $\theta_0 = 45°$, for different choices of target widths Δ_r and Δ_θ. As can be judged from the crosses superimposed on the kernels, the constructed averaging kernels match closely the specified target forms. The centre kernel has a radial width Δ_r of 0.0648 (fractional) solar radii and an angular width Δ_θ of 7.75°. This yields a standard error in the inversion of 3.3 nHz. Comparing this level of uncertainty with the range of the rotation rate observed at the Sun's photosphere (roughly 320 nHz – 460 nHz), or the range (approximately 300 nHz – 1500 nHz) of the rotation rate present in our artificial example (see Fig. 6a), it is evident that this is an acceptably small error for many purposes. The resolution could be squeezed further in either radius or latitude, but at the expense of increasing the standard error. Conversely, the error could be reduced somewhat by degrading the radial or latitudinal resolution.

A more complete picture of what may be achieved globally is provided by Fig. 3, which shows averaging kernels at various target radii and latitudes. These were all obtained with the same values of the scaling parameters $\alpha_r = 8.0$, $\alpha_\theta = 1.5$, as well as the same value of the error trade-off parameter $\mu_0 = 0.1$. As can be seen, the resolution is best in the outer part of the Sun, as expected from the asymptotic scalings (26), because modes with high l are sensitive to the rotation in these layers. The standard errors are also smallest in this region. The averaging kernels are very cleanly localized near the intended target location, for most locations in the outer half of the Sun. Only near the pole does the kernel exhibit noticeable nonlocal structure – only relatively low-m modes sample the region close to the pole, so it is harder to construct a kernel there. The standard error is also much higher for the near-polar inversion, for the same reason.

Even for target locations as deep as $0.4R$, the equatorial kernels are very well localized, and the error is only 4 nHz. The resolution could of course be improved further if the error was allowed to increase but, as illustrated in Fig. 2, one could not expect to improve the resolution substantially without at least doubling the standard error. The polar kernel at this radius shows considerable nonlocal structure, though it still has a main peak close to the intended location. Thus it is possible to localize kernels at different latitudes and thus to achieve latitudinal resolution at this depth, albeit with a considerable uncertainty σ. This is not the case at $r_0 = 0.1R$, our deepest target radius. Here all the kernels are similar and are localized at low latitudes. Nonetheless, apart from an obvious positive region in the convection zone, and a thin negative region near the surface at high latitudes, these kernels are reaonably well-localized. However, as discussed below, they depend heavily on the low-degree f modes in the Hare and Hounds dataset, which have so far not been observed.

To illustrate the importance of the $F_2^{nl}G_2^{lm}$, we have recomputed the coefficients used to construct the kernels in Fig. 3, setting $\beta_l = 0$ and $\zeta^{nl} = 0$ for all n and l. The values of all other parameters are unchanged. The results should still be superior to a basic $\mathbb{R}^1 \otimes \mathbb{R}^1$ inversion, as described at the beginning of Section 2, because we are choosing the coefficients $\widetilde{c}_l^m$ as a function of r_0 as well as of θ_0. As expected, we see in fig. 4 that neglecting the $F_2^{nl}G_2^{lm}$ contribution to the mode kernels has little effect in the outer part of the Sun, but degrades the kernels at $r_0 = 0.4R$ at all but the equatorial target. At the deepest target locations, the kernels constructed without taking $F_2^{nl}G_2^{lm}$ into account are very poor indeed. This is precisely as one would expect, because for such a deep target location the inversion needs to use low-degree (and, if they are available, low-frequency) modes, for which it is a poor approximation to neglect $F_2^{nl}G_2^{nl}$.

This point is further illustrated Fig. 5, where the radial coefficients c^{nl} are shown for two target locations, using the same parameters as for Fig. 3. Panel (a) shows coefficients for a target radius $r_0 = 0.7R$: in that case, the coefficients are approximately a function of lower turning point, as has been seen in 1-D inversions (Christensen-Dalsgaard et al. 1990). At $r_0 = 0.1R$ the low-degree f modes ($n = 0$) and gravest p modes are given most weight, as can be seen in panel (b). For such modes it is a poor approximation to neglect the $F_2^{nl}G_2^{lm}$ contribution to the mode kernels, which is

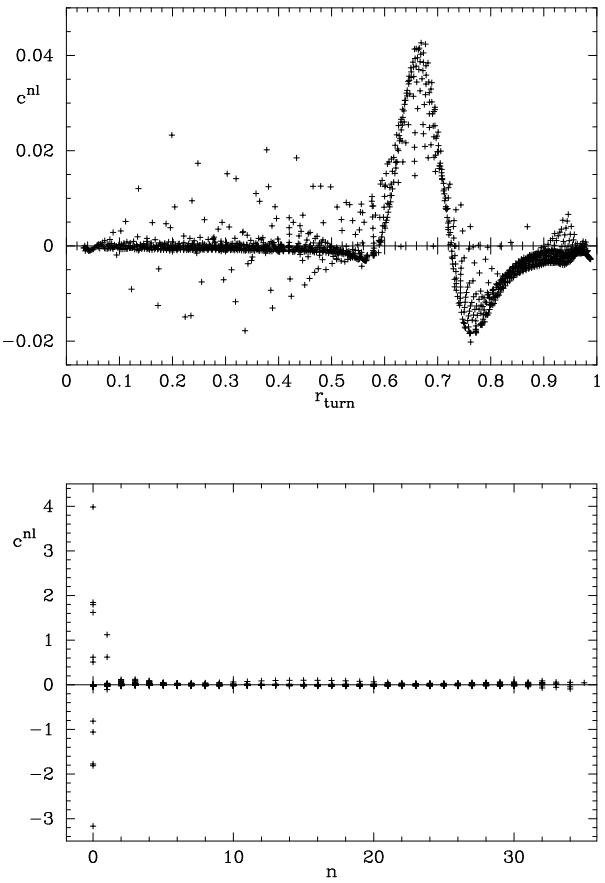

Figure 5 a. The coefficients c^{nl} for radius $r_0 = 0.7, \theta_0 = 45°$ as a function of turning point. b. The coefficients c^{nl} for $r_0 = 0.1, \theta_0 = 90°$ as a function of degree n

why the kernels in Figs. 3 and 4 differ so markedly for such deep target locations. It could be argued that the f modes should be excluded from the artificial data-sets because they have not yet been observed. It is clear that localizing a kernel as deep as $r_0 = 0.1R$ would then be more difficult since it is clear from fig. 5b that it is primarily these that are used in the localization this deep. At $r_0 = 0.4R$ the coefficients for the f modes are already of the same magnitude and smaller as all the other coefficients. Their omission should therefore not significantly affect the quality of the kernel nor the error magnification. It is clear from a comparison of figures 3 and 4 at $r_0 = 0.4R$ that the improvement with the new method proposed here is still appreciable, because of the improved treatment of the gravest p-modes.

Although the averaging kernels contain complete information about the resolution of an inversion, it is nonetheless instructive to see how well our method reconstructs a particular rotation profile. For this purpose, we have invented a rotation profile, shown in Fig. 6a. Its features include two jets, a fast-rotating core and polar region, and an enhanced rotation at $r \approx 0.9R$. Using the appropriate mode kernels, the rotation profile was then used to compute artificial splitting data D_{nlm}, which we then inverted using the same parameters as for Fig. 3. In the inversion, we assumed the error uncertainties described at the beginning of this section, but we performed two test cases, one where no

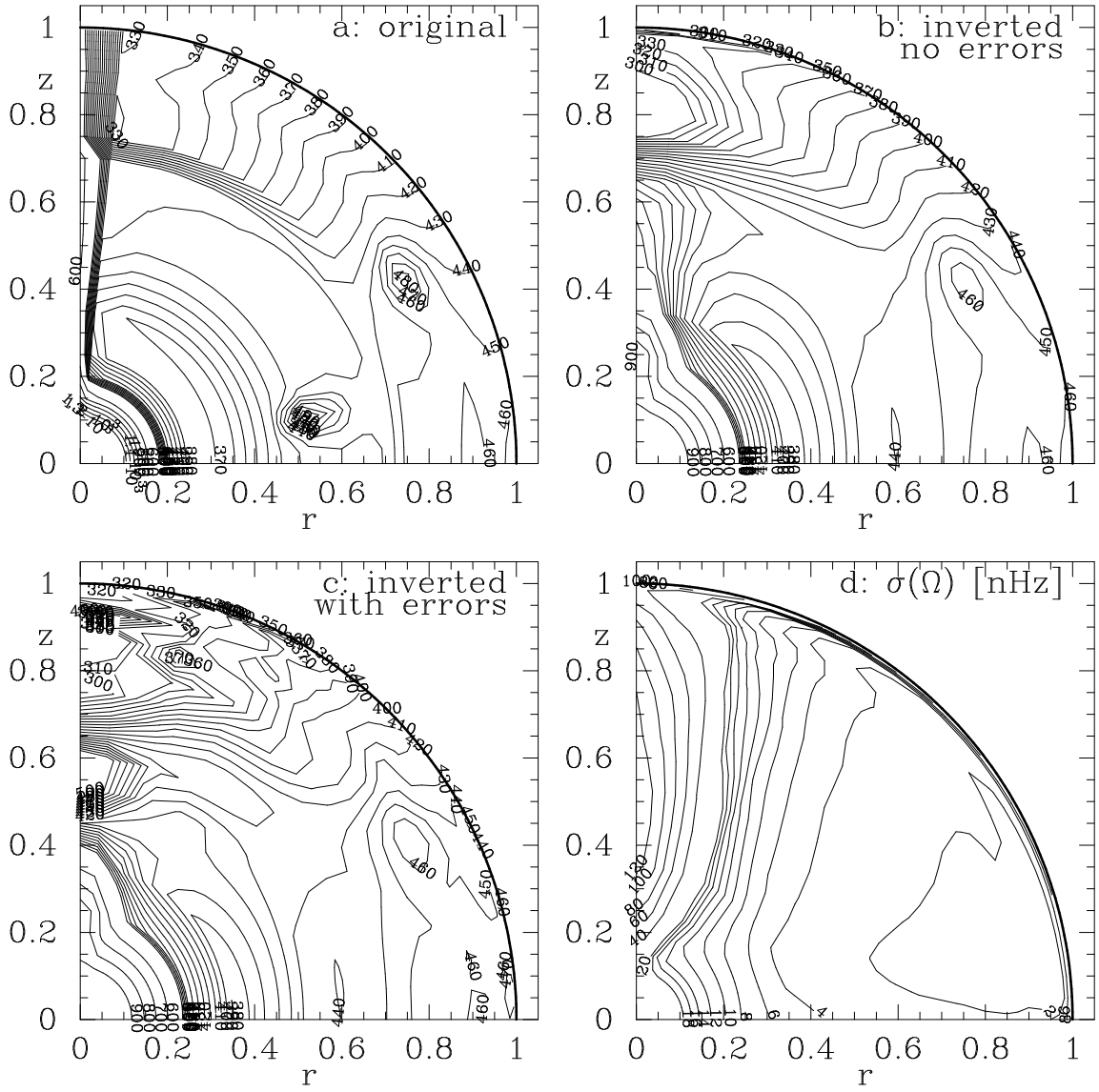

Figure 6 a. The original artificial rotation rate. b. The reconstruction using error-free data. c. The reconstruction with noisy data. d. The errors in the reconstructed rotation rate of c. The parameter vaues used in the reconstructions were $\alpha_r = 8.0$ $\alpha_\theta = 1.5$ and $\mu_0 = 0.1$.

errors were actually added to the data and a second where independent Gaussian errors with the assumed standard deviations were added as noise to the data. The inversion of the noise-free data is shown in Fig. 6(b). The fast-rotating core, the abrupt change in rotation at $r \approx 0.7R$ and the general trend of the rotation in the outer part of the Sun are all correctly inferred. The outer jet is rather poorly resolved, and the deeper jet is not convincingly detected at all. This is consistent with the width of the main peak of the averaging kernels shown in Fig. 3. In such a noise-free case, one could of course make much narrower kernels and hence obtain better resolution, because data errors are not a concern. However, the main purpose of showing the noise-free inversion is so that it can be compared with the inversion of noisy data in Fig. 6(c). Except near the pole, the corresponding contours in the two panels can very clearly be identified. The relatively small differences are due to the propagation of data errors, and are consistent with the standard errors quoted in Fig. 3 and with the contour plot of standard errors in Fig. 6(d). It is clear from panel (d) that the standard errrors increase substantially in the near-polar region, which accounts for the greater distortion of the noisy inversion near the pole. In the rest of the Sun, however, one can see from comparing panels (a)-(c) that it might be worthwhile to choose smaller widths for the averaging kernels, thus improving the resolution, even at the expense of somewhat greater errors. Fig. 7 illustrates that one could make a statistically significant detection of the deeper jet in

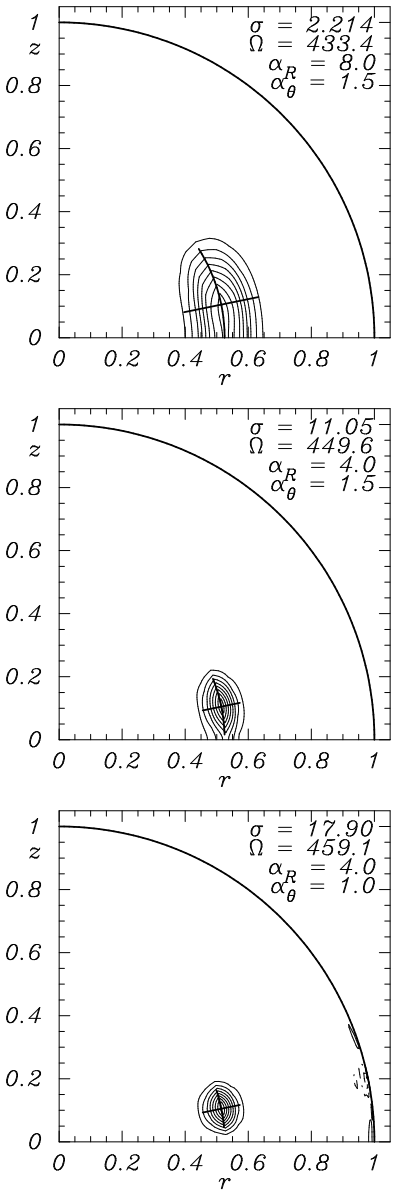

Figure 7 The effect of improved resolution on the error and the deduced rotation rate at the location of the 'jet'

this way.

Fig. 8 illustrates the difference between the inferred rotation from the noisy data and the true rotation profile divided by the standard error. In rather few places does the deviation between inferred and true rotation rise above 2σ. One place is the core, even though the inversion reproduces qualitatively the fast rotation. The other most significant deviations are around the two jets, particularly the deeper one. In the latter case, the broad averaging kernels have spread the jet out, so that not only is there a strong negative deviation where the prograde jet should have been, there is also a positive deviation around the jet where the inferred rotation is higher than the true rotation. Also shown in this figure are the locations where we constructed the inversion solution upon which the contour plots in Fig. 6 were based.

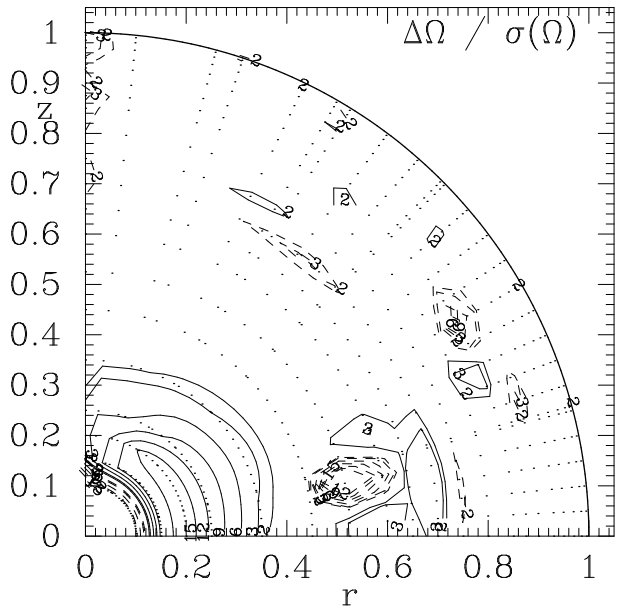

Figure 8 The difference between reconstructed and original, divided at each point by the local σ. Dots mark the central locations of all averaging kernels used in the reconstruction

4 DISCUSSION

We have previously demonstrated (PT1, PT2) that the SOLA method produces kernels that are of as good a quality as those obtained with the more traditional OLA formulations and shown that the SOLA method is computationally more efficient.

Our $\mathbb{R}^1 \otimes \mathbb{R}^1$ inversion differs from the one proposed by Sekii (1993a,b). He approximated each mode kernel as a product $F_1^{nl}(r)$ and $G_1^{nl}(\theta)$, where F_1^{nl}, G_1^{nl} are given by equations (5) and (8). The major difference of principle is that Sekii has thus approximated the kernels, whereas we keep the small term $F_2^{nl}G_2^{nl}$ and therefore make no approximation (beyond assuming that the rotational splitting is correctly described by first-order theory). Sekii's original method would not be recovered completely from ours in the limit $\beta_l \to 0$, $\zeta^{nl} \to 0$, because we do adjust latitudinal resolution as a function of depth which Sekii (1993b) already suggested but did not yet implement.

For all but the low degree modes (say $l \lesssim 5$), Sekii's approximation of neglecting F_2^{nl} should be very good. However, to perform inversions in the deep interior it is highly desirable to include the lowest degree modes, which penetrate deeply into the star, and this is apparently a drawback of Sekii's approximation (Sekii 1994). Now the effect on the inversion in the deep interior of neglecting the F_2^{nl} term is uncertain a priori, since even for low degree modes the F_2^{nl} component is not large compared to F_1^{nl}. However, from figures 3 and 4 it can be seen that there is a substantial difference between kernels at $r_0 = 0.1$ depending on whether or not the F_2G_2 terms are included. At this radius, the present method makes substantial use of the low-degree $n = 0$ modes (Fig 5). It could be argued that data for such modes are not available at present. But if they are observed

by e.g. GONG, they will be enormously helpful for probing the core region and it is highly desirable that our inversion methods make accurate use of them.

Apart from retaining the F_2G_2 term, and taking this into account in the latitudinal and radial localizations using SOLA, the present approach is very much in the same spirit as Sekii's original $\mathbb{R}^1 \otimes \mathbb{R}^1$ method (Sekii 1993a,b). Subsequently, Sekii has made a modification to the technique, to make a 2-D integral in the radial localization (Sekii 1993b, 1994). Such a modification might be included in our approach also.

Any multiple of $F_2^{nl}G_1^{lm}$ could be added into the first term on the right-hand side of equation (4) and maintain the form of the right-hand side, provided the same multiple was subtracted from the second term. In particular we could add $\zeta^{nl}F_2^{nl}G_1^{lm}$ to the first term and subtract it from the second. This is equivalent to replacing F_1^{nl} with $F_1^{nl}+\zeta^{nl}F_2^{nl}$ and replacing G_2^{lm} with $G_2^{lm} - \zeta^{nl}G_1^{nl}$. All such operations can be seen to be linear transformations of the vectors of functions $\mathbf{F}^{nl}$ and $\mathbf{G}^{lm}$. In the appendix it is shown that this always leads to the same inversion procedure provided that the two latitudinal target functions are equal up to a multiplicative constant. One implication of this is that our modified $\mathbb{R}^1 \otimes \mathbb{R}^1$ inversion cannot be obtained from a linear transformation of Sekii's method, since such transformations never lead to a radial inversion using just F_1^{nl} as Sekii's method does.

The advantage of both ours and Sekii's $\mathbb{R}^1 \otimes \mathbb{R}^1$ technique for SOLA type inversions is that it is never necessary to invert a matrix with a dimension of the order of the total number of frequency splittings (i.e. ~ 70000). The largest matrix to invert for construction of the latitudinal averaging kernels is l_{max} which is 250 for the mode set under consideration. For the radial averaging kernels it is in principle the number of different n, l-combinations which is 1380 for the Hare and Hounds mode set. However the number of modes for the radial inversions can be reduced by projection onto a suitable basis after performing an SVD reduction (cf. PT1; Christensen-Dalsgaard & Thompson 1993) to 87.

Matrix inversion is an $\mathcal{O}(N^3)$ process and therefore naively the speed-up of the inversion due to the technique described here for this mode set would be a factor close to :

$$\left(\frac{\sum\limits_{l\in\mathcal{M}} \left[N_m(l)^3\right]}{69662^3} \right)^{-1} \approx 3 \times 10^6 \,, \tag{36}$$

where $N_m(l)$ is the number of observed modes with distinct m values for each l. However the integrations in the calculation of the vector $\mathbf{v}$ in (36) turn out to dominate in the computing time and this is an $\mathcal{O}(N)$ process so the overall speed up is more modest. Taking into account that the full 2-D inversion would require computing 2-D integrals in the determination of $\mathbf{v}$ in (36) instead of 1-D integrals the theoretical speed up is a factor of $\sim 14 \times 500 = 7000$. Here 500 is the approximate number of grid points in the radial direction which one would also have to integrate over in computing a complete 2-D integral (to resolve the mode kernels adequately), and which can now be omitted in all 1-D latitudinal inversions. Since there is an integration for each mode there is an extra factor 14 from the ratio of the number of modes used in the 2-D and $\mathbb{R}^1 \otimes \mathbb{R}^1$ inversion :

$$\left(\frac{\sum\limits_{l\in\mathcal{M}} N_m(l)}{69662} \right)^{-1} \approx 14$$

This estimate of the speed-up was not experimentally tested.

Finally it should be noted that a very preliminary version of this method was used in the GONG Hare and Hounds exercise (Gough & Toomre, 1993). The results there were poorer than those presented here, since the weighting factors ζ^{nl} and the scheme for obtaining the optimal resolution at all radii had not been satisfactorily developed at that time. The quality of the results is sensitive to these choices.

ACKNOWLEDGMENTS

Much of the work undertaken in this paper was performed while FPP was supported by grant GR/H33596 from the UK Science & Engineering Research Council.

REFERENCES

Backus, G. E., Gilbert, J. F., 1968, Geophys.J., 16, 169
Backus, G. E., Gilbert, J. F., 1970, Phil.Trans.R.Soc.Lond.A, 266, 123
Christensen-Dalsgaard, J., Thompson, M. J., 1993, A&A 272, L1
Dziembowski, W. A., Goode, P. R., Pamyatnykh, A. A., Sienkiewicz, R., 1994, ApJ 432, 417
Gough, D. O., 1985, Sol.Phys. 100, 65
Gough, D. O., Toomre, J., 1993, Global Oscillation Network Group, Report No. 11 (National Optical Astronomy Observatories, National Solar Observatory, Tucson).
Pijpers, F. P., Thompson, M. J., 1992, A&A 262, L33 (PT1)
Pijpers, F. P., Thompson, M. J., 1994, A&A 281, 231 (PT2)
Schou, J., Christensen-Dalsgaard, J., Thompson, M. J., 1990, ApJ 385, L59 (SCDT)
Sekii, T., 1993a, in Brown T. M., ed., Proc. GONG 1992: Seismic investigation of the Sun and stars, PASPC, 42, 237
Sekii, T., 1993b MNRAS, 264, 1018
Sekii, T., 1994 MNRAS, submitted
Thompson, M. J., 1993, in Brown T. M., ed., Proc. GONG 1992: Seismic investigation of the Sun and stars, PASPC, 42, 141

APPENDIX A: INVARIANCE OF KERNELS UNDER LINEAR TRANSFORMATIONS

The 2D $\mathbb{R}^1 \otimes \mathbb{R}^1$ splitting of the kernels of equation (4) is invariant under any linear transformation. The transformations of the vector of functions $\mathbf{F}$ is written as :

$$\begin{pmatrix} \widetilde{F}_1 \\ \widetilde{F}_2 \end{pmatrix} = \begin{pmatrix} o & p \\ q & r \end{pmatrix} \begin{pmatrix} F_1 \\ F_2 \end{pmatrix} \,, \tag{A1}$$

and the transformation of the vector of functions $\mathbf{G}$ as :

$$\begin{pmatrix} \widetilde{G}_1 \\ \widetilde{G}_2 \end{pmatrix} = \begin{pmatrix} a & b \\ c & d \end{pmatrix} \begin{pmatrix} G_1 \\ G_2 \end{pmatrix} \,, \tag{A2}$$

which covers all the transformations considered in this paper. The inner product of the $\mathbf{F}$ and $\mathbf{G}$ vector should not be affected by the transformation, therefore

$$\widetilde{\mathbf{F}} \cdot \widetilde{\mathbf{G}} = \begin{pmatrix} F_1 \\ F_2 \end{pmatrix}^T \begin{pmatrix} o & q \\ p & r \end{pmatrix} \begin{pmatrix} a & b \\ c & d \end{pmatrix} \begin{pmatrix} G_1 \\ G_2 \end{pmatrix} \tag{A3}$$

must be equal to :

$$\begin{pmatrix} F_1 \\ F_2 \end{pmatrix}^T \begin{pmatrix} G_1 \\ G_2 \end{pmatrix} \ . \tag{A4}$$

As a consequence of this it is clear that the two matrices must be each others inverse :

$$\begin{pmatrix} o & q \\ p & r \end{pmatrix} \ = \ \frac{1}{(ad-bc)} \begin{pmatrix} d & -b \\ -c & a \end{pmatrix} \tag{A5}$$

The single kernel used for the radial inversions is F_R :

$$F_R \ \equiv \ F_1 + \zeta F_2 \tag{A6}$$

Here the constant ζ is the ratio of the values of the kernels $\mathcal{G}$ evaluated at the target location $u = u_0$. In the formulation used in the main text

$$\zeta = -\left(\frac{\nu_{\min}}{\nu}\right)^2 \tag{A7}$$

In the transformed set

$$\widetilde{\zeta} = \frac{(c+\zeta d)}{(a+\zeta b)} \tag{A8}$$

In this case the new radial kernel $\widetilde{F}_R$ becomes

$$\begin{aligned} (a+\zeta b)\widetilde{F}_R \ &= \ \frac{1}{(ad-bc)}\left[(a+\zeta b)(dF_1 - cF_2)\right. \\ &\qquad \left. +(c+\zeta d)(-bF_1 + aF_2)\right] \\ &= \ F_1 + \zeta F_2 \end{aligned} \tag{A9}$$

The factor $(a+\zeta b)$ on the left-hand side drops out again because of the subsequent normalization of the kernels. The radial part of the inversion therefore is not affected by the linear transformation. The latitudinal part of the inversion does appear different but if the two components of the target function are equal up to a constant factor of multiplication for the original set (G_1, G_2), then the transformation will preserve that and therefore also the inversion.
The original method as described in the paper by Sekii (1993b) which uses the radial kernel $F_R = F_1$ is not obtainable from an invertible linear transformation of the kernels.